2019 International Conference on Unmanned Aircraft Systems (ICUAS)
Atlanta, GA, USA, June 11-14, 2019

Exploiting Ground and Ceiling Effects on Autonomous UAV Motion Planning

Shijie Gao[1], Carmelo Di Franco[1], Darius Carter[2], Daniel Quinn[2], and Nicola Bezzo[1]

***Abstract*— Micro Aerial Vehicles (MAVs) and in particular quadrotors have gained a lot of attention because of their small size, stable, robust, and diverse sensing capabilities that make them perfect test beds in several safety critical operations. Shrinking these vehicles is desirable since agility increases. However, it entails smaller power sources and hence less flight time. Adding sensors on these systems also implies more energy consumption due to both the added weight and the supplied energy to the sensors. In this work, we build a framework to leverage the flow dynamic effects near surfaces to recognize grounds and ceilings during operations and to plan a trajectory while minimizing energy consumption. Our proposed framework leverages data from real experiments to model the behavior of the system near surfaces and graph theoretical approaches for energy efficient motion planning. As a result, this study indicates that *i*) we can detect surfaces during operations without the need of extra onboard sensors and *ii*) we can minimize energy consumption up to 15% when the system can fly near ground or ceiling surfaces. The proposed framework is validated with experimental results on a quadrotor UAV.**

I. Introduction

Unmanned Aerial Vehicles (UAVs) have become very popular in recent years due to the myriad of purposes in which they can be deployed that span both military and civilian applications. One special class of UAVs is Micro Aerial Vehicles (MAVs), which are vehicles that have size restrictions and are by far the most common UAVs, thanks to their lower cost and multidisciplinary use. They are often research-driven and can easily have applications in commercial, government, military, and hobbyist domains. Among MAVs, multirotors – in particular quadrotors, the subject of this paper – have gained a lot of attention due to their maneuverability, agility, payload potential, and stability.

One major issue common to all of these platforms is that they are not energy efficient. Their battery life is short and is often the main factor limiting deployment in real-world applications. Adding payloads such as sensors further decreases their mission time due to the increase in weight and energy consumption associated with the operation of the added device.

In this work, we propose a novel approach that leverages the flow dynamics near surfaces like the ground and ceiling to 1) sense the environment and/or 2) exploit these effects for performing energy efficient motion planning.

[1] Shijie Gao, Carmelo Di Franco, and Nicola Bezzo are with the Departments of Systems Engineering and Electrical and Computer Engineering, University of Virginia, Charlottesville, VA 22904, USA {sg9dn, cd8gm, nbezzo}@virginia.edu

[2] Darius Carter and Daniel Quinn are with the Departments of Mechanical and Aerospace Engineering, University of Virginia, Charlottesville, VA 22904, USA {djc3xy, dbq9d}@virginia.edu

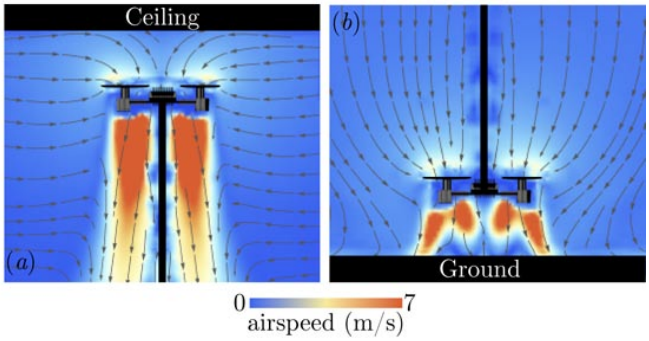

Fig. 1. The flow field surrounding a quadrotor UAV near ceiling (*a*) and ground surfaces (*b*). In (*a*) the flow field is perturbed by the ceiling; streamlines above the rotors become horizontal and downwash is reduced. Arrows show streamlines interpolated from a Stereo Particle Image Velocimetry vector fields. In (*b*) the flow field is perturbed by the ground; jets beneath the rotors stagnate and downwash is reduced.

When a UAV flies near ground or ceiling (Figs. 1 and 2), it experiences an increase in lift. This lift increase represents a decrease in the thrust required to keep the UAV aloft and thus a decrease in energy consumption. For example, in agriculture operations, a UAV could fly low to the ground to reduce energy consumption, especially over long distances. In indoor environments, a UAV could fly close to the ceiling, avoiding crowds and objects while also consuming less energy.

A secondary desired effect is that by monitoring thrust, the UAV can detect the distance to nearby surfaces and prevent collisions. This latter effect is especially beneficial in environments where sensors may not be able to estimate the distance from the ground/ceiling. For example, in a dusty environment like a desert, a conventional camera, sonar, or lidar-based sensor may fail to detect obstacles, which may lead to crashes as a vehicle is landing.

Fig. 2. An AscTec Hummingbird flying close to a ceiling.

Authorized licensed use limited to: University of Virginia Libraries. Downloaded on February 19,2022 at 19:12:14 UTC from IEEE Xplore. Restrictions apply.

With these considerations in mind, in this paper, we build a framework for quadrotor UAVs to exploit ground and ceiling effects to detect surfaces and create energy efficient motion planning. To this end, we propose 1) an experiment-driven analysis of flow dynamical effects using our testbed of quadrotor UAVs, 2) a model for sensorless autonomous landing via surface detection, and 3) a method for using our models to construct a special graph to perform energy efficient motion planning that leverages ground and ceiling effects by using a Dijkstra's algorithm to obtain the minimal energy route.

Our results are validated by experimental results on a quadrotor testbed. The experiment validates that the proposed surface detection method enables the quadrotor to land safely on the ground or the obstacle surface without the assistance of extra sensors. The energy-efficient path can save up to around 10% of energy.

Different from other related works here together with extensive analysis on the ground and ceiling effects we propose a motion planning framework that leverages these effects both to detect surfaces during run-time and perform autonomous navigation while minimizing energy consumption. To the best of our knowledge, this is the first work that attempts to leverage near-surface effects for sensing and motion planning.

II. Related Work

In the literature we find several works dealing with aerial vehicle near-surface effects both from the flow dynamics and robotics perspectives.

Classic momentum theory predicts that lift increases by a factor of $(1-(4\hat{z})^{-2})^{-1}$, where $\hat{z}$ is the ceiling/ground proximity normalized by rotor radius [1]. This relation is derived for single-rotor helicopters in forward flight and assumes that viscous effects are negligible and that $\hat{z} > 0.5$. Recent work has shown that the theory overpredicts ceiling effects [2] and underpredicts ground effects [3], [4] when applied to small quadrotors. In response, authors in [5] recently proposed a modification to the classic Cheeseman-Bennett theory [1]. Using an inviscid control volume argument based on uniform incoming streamlines, they proposed that lift increases by a factor of $\sqrt{1+\frac{1}{8}\hat{z}^{-2}}$. Sanchez et al. [6] modified the Cheeseman-Bennett theory to include four point sources (one for each rotor) instead of one, and they empirically fit the new model to their data. It remains unclear how well these old and new models scale to different-sized quadrotors, and how lift scales differently near the ceiling versus near the ground. This gap in understanding has prompted us to take a look at the flow field in conjunction with lift forces to better understand the ground effect.

Ground and ceiling effects have been used actively in many robotics applications. In [7], the authors leverage the ceiling effect to perform bridge inspection by maintaining in contact a specially designed UAV to the ceiling. Authors in [8] exploited the ground effect to perform a blind terrain mapping while [9] treated the near-surface effects as disturbances in order to improve multi-floor navigation and mapping inside buildings. In [10], the authors take into account the ground effect to improve the altitude controller of a helicopter approaching the ground. In particular, the authors adapt in real time the gains of the collective controller and the engine gas controller according to the current height of the vehicle.

Although ground and ceiling effects have been actively used in many applications such as the ones described above, they have never been used for detecting near surfaces and for motion planning. For instance, it could be possible to detect the presence of the ground or the ceiling and leverage this information for collision avoidance or autonomous landing. Indeed, autonomous landing is currently performed using sensors such as cameras, ultrasonic sonars, IMU, GPS, optic flow, and Barometric pressure sensors [11]. These approaches, however, may require computational capabilities or heavier payloads, which are challenging in small-sized UAVs. Moreover, some sensors may be malfunctioning or could be inaccurate in harsh conditions such as low-light and dust.

This work proposes a sensorless surface detector that leverages the thrust reduction occurring when approaching a surface. The surface detector can be used for collision avoidance or autonomous landing. Additionally, the thrust reduction can be used to reduce energy consumption and increase flight time. For instance, in [7], the authors observed an increase in the maximum flight time of the UAV while being in contact with the ceiling. From a path-planning point of view, some algorithms minimize energy consumption by monitoring and re-planning based on wind disturbances [12] and by setting an optimal speed along the path [13]. While roboticists have studied path planning approaches that leverage characteristics of the environment, ground and ceiling effects are not typically exploited for navigation purposes. Based on these considerations, in this work, we propose a surface-based energy-efficient path planning algorithm that exploits the thrust reduction near surrounding surfaces to detect surfaces and minimize energy consumption.

III. Problem Formulation

In this work, we are interested in leveraging thrust reduction near surfaces to sense the distance to a surface and achieve optimal energy path planning for a UAV. Specifically, two main problems are investigated in this work:

Problem 1: **Surface Detection.** Consider a UAV unable to estimate its distance to the ground or the ceiling due to a lack of onboard sensors or possible malfunctioning on the existing sensors. Given the thrust F of the UAV, the objective is to

- find a function f which maps the thrust values to the distance from the surface such that $d = f(F)$;
- detect the surface s and its distance d from the UAV in order to avoid collisions and replan accordingly.

Note that the problem above is concerned with the detection of ceilings and grounds. Wall effects, as we will show later, are negligible by leveraging flow dynamics and thus will not be considered in this paper. Two functions – one for ground and the other for the ceiling effects – that map thrust to the distance to a surface will be extracted and used to build a surface detector. The specific case study that will be considered here to validate our approach is an autonomous detection of surfaces during landing which is the most typical

Authorized licensed use limited to: University of Virginia Libraries. Downloaded on February 19,2022 at 19:12:14 UTC from IEEE Xplore. Restrictions apply.

application where this approach will have a direct impact. Both functions together with energy considerations on UAV motion planning will be used to solve the next problem.

Problem 2: **Surface-based Optimal Path Planning.** A UAV has the objective to reach a goal p_g starting from p_0 by navigating through a predefined path $P = \{p_0, p_1, \ldots, p_N, p_g\}$ consisting of N intermediate waypoints in the presence of different types of surfaces. Given the model obtained by solving *Problem* 1, our goal is to find a policy to plan the minimum energy trajectory between the initial position of the vehicle and the final goal. Formally, given a predefined path P and a set of intermediate surfaces S whose positions are assumed to be known a priori, find a policy to generate a directed graph $G(V, E)$ with a set of vertices $v \in V$ and edges $e \in E$ and compute the weights w associated to each edge e by using the model obtained by solving *Problem* 1 in order to obtain the shortest energy path to reach the goal along the graph G.

IV. Ground and Ceiling Effects

A. Measuring tethered lift and flow fields

To investigate how ground and ceiling surfaces affect the quadrotor lift, we built an arena to measure flow fields around quadrotors (Fig. 3*a,b*). Compared to other studies, our testing apparatus allows uniquely small $\hat{z}$ values and the ability to directly capture the flow fields governing ground and ceiling effects. The arena is a $1.5 \times 1.5 \times 1.5$ m cube made out of glass and black plastic. A custom traverse raises/lowers quadrotors to a user-defined height, z, defined as the distance between the propeller midline and the ground/ceiling. Following others [1], [2], [5], we nondimensionalize height by rotor radius: $\hat{z} \equiv z/r$. For this study, we used a small quadrotor (Crazyflie 2.0, $r = 23$ mm) so that we could map the full flow field while measuring forces simultaneously. We hypothesize that similar lift scalings would apply to larger quadrotors with similar form factors, which we confirm in Section V.C. The Crazyflie was suspended from the traverse by a steel rod (radius 0.64 cm), with an in-line 1-kg load cell (Omega LCFD - 1kg). We measured time-averaged lift for 5 throttle levels (0%, 25%, 50%, 75%, and 92% (max)) at 20 distances from the ground/ceiling. The traverse automatically visited each distance 15 times in a randomized order. The 0% case was subtracted from all others to give the difference between lift and weight, or "net lift", L. To facilitate comparisons between cases, we calculated the percent increase of net lift near the ground/ceiling, that is, its value divided by its value when far from the wall: L/L_∞.

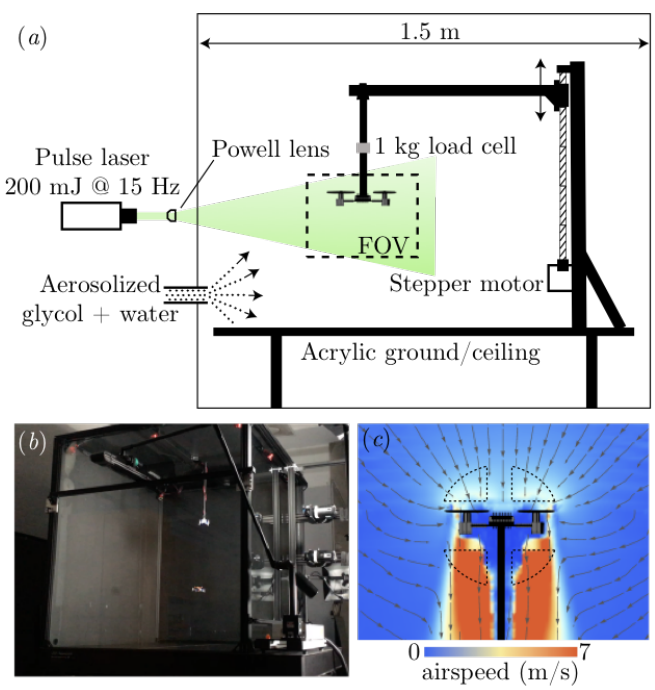

Fig. 3. *a*) A Crazyflie was suspended in a $1.5 \times 1.5 \times 1.5$ m glass and HDPE cube. We used Stereo Particle Image Velocimetry (SPIV) to map time-averaged flow fields and a load cell to measure lift near the ceiling/ground. *b*) A photograph of the arena shows the Powell lens that creates the laser sheet (top left) and the two high speed cameras (right). *c*) SPIV data far from the ceiling/ground show suction zones above the rotors and high speed jets beneath the rotors. The dotted lines are zones used to estimate downwash.

To measure flow motion around the Crazyflie, we used Stereo Particle Image Velocimetry (SPIV) to track neutrally buoyant particles in the arena. The SPIV system uses a dual-cavity pulse laser (Litron, 200 mJ @ 15 Hz) to illuminate aerosolized particles of glycol and water (diameter 14 μm). Particle motion is triangulated by two high-speed cameras (Phantom SpeedSense M341, 4MP) that feed into cross-correlation software (Dantec Dynamic Studio). Based on a convergence test, we determined that 150 image pairs were sufficient for time-averaged velocity fields to converge to $< 0.1\%$ average projection error per 10 μm. The result of the averaged cross-correlations is a 32×32 px grid of velocity vectors, which we used to plot airspeed density plots and trace streamlines.

B. Lift and flow fields: results versus theory

For each throttle level, we found that net lift increases as the Crazyflie approaches the ground or ceiling (Fig. IV-B*a,b*). The effect was especially pronounced near the ceiling, where lower allowable $\hat{z}$ values lead to a nearly 60% increase in lift. Lift did not change considerably near sidewalls (Fig. IV-B*c*), so we focused on ground/ceiling effects. The percent increase in net lift near the ground/ceiling (L/L_∞) appears to be similar for each throttle value (Fig. IV-B*c*), demonstrating that similar lift increases would be observed regardless of payload. Classic momentum theory predicts the same inverse relationship for both near-ceiling and near-ground lift: $L/L_\infty = 1/(1 - (4\hat{z})^{-2})$ [1]. While our data show qualitatively similar behavior, we observed different scalings for the lift near the ground and lift near the ceiling (Fig. IV-B*c*). The model – which is derived for helicopters – assumes a point source for the rotor, an assumption that breaks down for small $\hat{z}$. Indeed, classic theory seems to predict near-ceiling lift well at high $\hat{z}$ values, but overpredicts near-ceiling lift for $\hat{z} < 1$ (Fig. IV-B*c*). Conyers et al. [2] saw a similar overprediction, also starting around $\hat{z} = 1$. We found that a simple inverse power law ($a/\hat{z}+b$) showed good agreement (R^2 >0.96) compared to the classic momentum theory model.

Motivated by the deviation from classic momentum theory, we used Stereo Particle Image Velocimetry (SPIV) to map

Authorized licensed use limited to: University of Virginia Libraries. Downloaded on February 19,2022 at 19:12:14 UTC from IEEE Xplore. Restrictions apply.

the airflow around the Crazyflie. In the case where no boundaries are nearby ($\hat{z} \gg 1$), the Crazyflie produces smooth suction zones above the rotors and high-speed turbulent jets beneath the rotors (Fig. 3*c*). Near the ceiling, streamlines above the rotors become more horizontal, and the jets beneath the rotors reduce in strength (Fig. 1*a*). Near the ground, the jets stagnate beneath the rotors, presumably creating a region of high pressure (Fig. 1*b*). In general, the presence of the ceiling and ground reduces the downwash caused by rotors. Based on linear momentum theory one would predict the downwash near the ceiling/ground to be $u_\infty(1-(4\hat{z})^{-2})$, where u_∞ is the downwash far from the ground/ceiling [1]. The velocity in the rotor plane is obscured, so we estimated downwash by averaging four regions above and below the rotors (Fig. 3*c*). In the near-ground and near-ceiling cases, we calculated downwash to be $0.94u_\infty$ (ceiling) and $0.78u_\infty$, compared to $0.993u_\infty$ and $0.996u_\infty$ predicted by Cheesman-Bennett Theory and $0.996u_\infty$ predicted by a modified ceiling theory [5]. The theories are developed for helicopters, where the Reynolds number based on rotor diameter is much larger ($Re \equiv 2u_\infty r/\nu = \mathcal{O}(10^6)$ versus $\mathcal{O}(10^3)$; ν is kinematic viscosity). Viscous effects must, therefore, play a role near the ground; our downwash data suggest improved models for small quadrotors near boundaries are necessary. Nevertheless, motivated by our empirical fit, we used an inverse power-law ground/ceiling model to test freely flying quadrotors in this study.

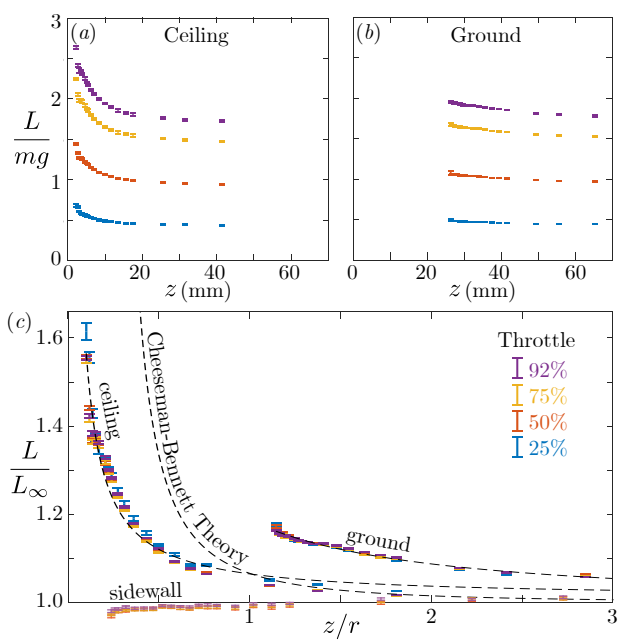

Fig. 4. *a,b*) The net lift (L) scaled by body weight (mg) increases near the ceiling (*a*) and ground (*b*). Net lift shows a slight decrease near sidewalls. *c*) The percent increase in net lift near boundaries shows an inverse relationship with dimensionless height: $L/L_\infty = a/\hat{z} + b$ (ceiling, $a = 0.055$, $b = 1.01$; ground, $a = 0.0198$, $b = 0.989$) Linear momentum theory [1] predicts predicts $L/L_\infty = 1/(1-(4\hat{z})^{-2})$ using a sink/source mirrored beneath the ground/ceiling. Throttle is percent of max thrust (≈ 0.4 N).

C. Ground and Ceiling effects Characterization

When a quadrotor is close to a surface, it benefits from an increased lift, i.e., the thrust required for hovering decreases. To further characterize such a behavior, we performed a set of experiments by flying an untethered quadrotor at different distances from the ground and a ceiling surface.

For our testbed, we used an AscTec Hummingbird quadrotor UAV controlled using the Robot Operating System (ROS). The experiment is performed indoor in order to capture the motion of the quadrotor with high precision through the use of a VICON motion capture system. A 1.8 m by 0.9 m PVC transparent board is placed at the height of 1.95 m and used as ceiling surface. Fig. 5 shows the experimental setup with the quadrotor hovering at mid-distance from the ground and the PVC ceiling.

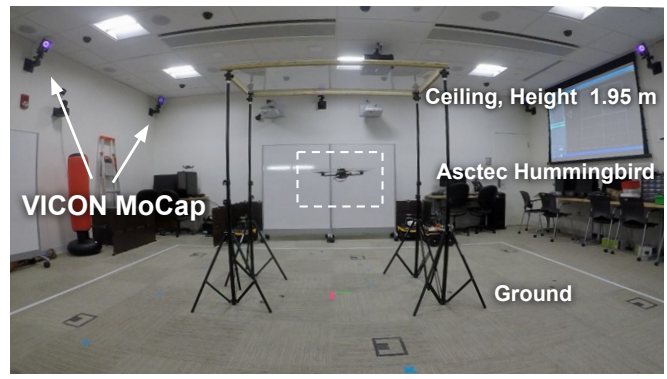

Fig. 5. Experiment setup for validating ground effect and ceiling effect.

We performed two experiments to characterize the impact of the ground and ceiling effects on the thrust given to the quadrotor and to confirm the results presented in the previous section. In the first experiment, the quadrotor hovers for 10 s at 12 different positions from the ground and ceiling, respectively. For each distance, we collected the throttle given to the UAV.

In the second experiment, we measured the throttle during an ascending trajectory from the ground to the ceiling surfaces, and vice-versa without stopping at intermediate points. We repeated the ascending and descending trajectories 5 times.

Fig. 6 shows the measured throttle (point clouds) as a function of the distance from the ground and ceiling for both the hovering and the descending/ascending cases. As discussed in the previous section, we fit the collected data with a power model, that in our case was found to have the following form:

$$T_t = a \cdot d_t^b + c \tag{1}$$

where d_t denotes the distance to the ground at time t and T_t represents the thrust at time t. Table I summarizes the parameters of eq.(1) for the fitted curves presented in Fig. 6.

As expected, there is a significant throttle reduction in all the experiments. Similarly to the results presented in the previous section, the ceiling effect in hovering state (Fig. 6b) starts appearing sooner than the ground effect(Fig. 6a) when approaching the surface(around 0.5 m). Furthermore, as expected, the throttle when descending (ascending) (Fig. 6c,

Authorized licensed use limited to: University of Virginia Libraries. Downloaded on February 19,2022 at 19:12:14 UTC from IEEE Xplore. Restrictions apply.

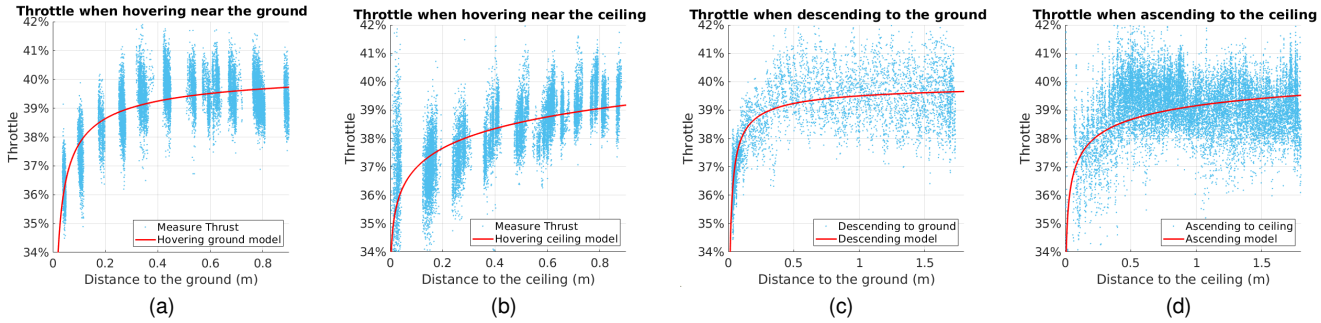

Fig. 6. Ground and ceiling effects when hovering, descending, and ascending. (a) Ground effect when hovering: The quadrotor hovers for 10 seconds at a multiple distances. The maximum throttle reduction is 9.26% at 3 cm from the ground. (b) Ceiling Effect when hovering: the maximum reduction on throttle is 9.03% at 4 cm from the ceiling. (c) Ground effect when descending: the maximum reduction on throttle is 8.72%. (d) Ceiling effect when ascending: The maximum reduction is 7.96%.

TABLE I
PARAMETERS FOR MODELS

Maneuver Type	Parameters		
	a	***b***	***c***
Hovering ground	-0.00858	-0.52510	0.4063
Hovering ceiling	0.39280	0.02637	0.0
Descending	-0.00539	-0.57980	0.4004
Ascending	-0.03474	-0.19050	0.4263

Fig. 6d) is slightly less (more) than the thrust when hovering since a different thrust is needed when the UAV moves. Note also that the reason why the a and b parameters are positive in the hovering near the ceiling case is due to the bias c that was found to be 0 only in that case.

The results presented above confirm the analysis provided in Section IV-A. The maximum thrust reduction from these experiments is 9.63% obtained by hovering at 5 cm above the ground. In the previous section, we recorded a 60% reduction because it was possible to move the CrazyFlie propellers up to a few millimeters away from the surface since it was tethered. If we scale the x-axis in Fig. 6 by dividing the distance to the propellers' radius (9.8 cm), we obtain curves that are in line to the values observed in Fig. IV-B.

V. GROUND AND CEILING DETECTION

This Section aims to solve the second portion of *Problem* 1, i.e., leveraging the model that we have just built to detect surfaces above or below the UAV. As we mentioned in the introduction, typical sensors used for distance detection may not work in harsh scenarios such as low illumination or under high dust concentration conditions. Furthermore, Micro aerial vehicles may not have enough computational resources for running vision-based approaches or may be unable to add sensors due to payload restrictions. In this section, we propose a three-stage surface detection method that can be used for collision detection and avoidance from ground and ceiling surfaces. We focus on the application of autonomous sensorless landing for ease of discussion; however, the same approach applies to ceil detection, too. Our approach will be validated by a set of experiments in which an autonomous landing procedure onto an unknown surface height is performed.

A. Methodology

The proposed three-stage algorithm for autonomous sensorless surface detection and landing is summarized in Fig. 7. Depending on if the quadrotor is descending or hovering, we use the descending and hovering model, respectively, computed in the previous section to estimate the distance from the ground.

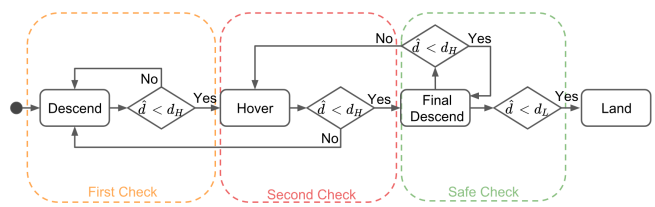

Fig. 7. State machine for the ground detection and landing procedure. The procedure includes three stages to guarantee the safety of quadrotor while landing.

In the first stage, the UAV keeps descending and continuously checks if the estimated height $\hat{d}$ is less than a designed threshold d_H. The threshold is chosen considering that the ground effect starts becoming visible when the distance from the surfaces, $d < 0.4$ m. In our implementations we set a threshold of $d_H = 0.25$ m. If the estimated distance is below the threshold, the UAV enters stage two in which it hovers for δt time in order to confirm or disregard the estimated height. This second stage is introduced to identify if the detected reduction on thrust in the first stage is due to the surface effect or noisy measurements. In our experiments, we picked $\delta t = 1$ s in order to have enough time to collect throttle measurements while hovering. If the recorded estimate is above the threshold, the algorithm returns to stage 1, and the UAV keeps descending. Otherwise, the UAV enters stage three and begins the final descending/landing procedure. In this stage, the quadrotor descends until the estimated distance is below the desired landing height d_L The desired landing height is chosen to guarantee that turning off the rotor will not damage the quadrotor at that height. In our implementations $d_L = 0.05$ m. If an abnormal estimated height is detected during the landing stage, the quadrotor returns to the hovering stage (stage 2) where it stops again for δt in order to double check its estimation.

Authorized licensed use limited to: University of Virginia Libraries. Downloaded on February 19,2022 at 19:12:14 UTC from IEEE Xplore. Restrictions apply.

Similar to ground detection, the UAV can use the ascending model (Fig. 6d) and the hovering ceiling model (Fig. 6b) to estimate the distance from the ceiling. The ceiling detection can help the quadrotor avoid collision with the surface above without using any added sensors.

B. Experiment validation

To validate the floor detecting method, we have used an AscTec Hummingbird quadrotor. The experiment setup is similar to the experiment in section IV-C. We used ROS to control the quadrotor and the VICON motion capture system to get the ground truth of the quadrotor's position. The throttle was measured at the frequency of 100 Hz, with the quadrotor descending at a speed of 0.1 m/s. The position control algorithm loop was run at a frequency of 10 Hz. In order to reduce the noise in the estimation, we applied a window filter with size $w = 40$ values to the throttle measurements. The window's size has been chosen considering the sampling frequency and the quadrotor descending speed. With the chosen window size, the delay produced by the filter is about 0.4 s, meaning that the quadrotor will have a displacement up to 4 cm before the surface is detected.

The estimated height from the ground is computed as:

$$d_t = \exp(\frac{\overline{T_t} - a}{b \cdot c}) \tag{2}$$

where a, b, and c are the model parameters given in Table I and $\overline{T_t}$ is defined as:

$$\overline{T_t} = \sum_{t-w}^{t} \frac{1}{w} T_t. \tag{3}$$

Multiple experiments were conducted in which the quadrotor performed an autonomous landing starting from a hovering height of 1.75 m. Fig. 8b zooms in the final period of landing on the ground while Fig. 8a shows multiple snapshots of the real experiment. The quadrotor enters in the first stage and slowly descends checking if the estimated altitude is below the threshold $d_H = 0.25$ m. In this first part of the mission, when the quadrotor is far from the ground, it is not possible to discriminate the height since the mean thrust is constant. As the quadrotor gets close to the ground, the estimated distance to the surface is converging to the real distance. At 28.73 s, the estimated distance is less than the threshold and the quadrotor starts hovering for 1 s to double-check the estimated distance. At 29.78 s, the quadrotor confirms that its height is less than d_H from the surface and moves to the third stage. In the last part of the mission, the quadrotor keeps slowly descending until the estimated distance is less than $d_L = 0.05$ m at which point its motors are turned off. From the experiments, it is possible to note that, as expected, for distances greater than 0.4 m, the estimation is not precise. However, when reaching the surface, the estimated distance is close to the real one. Note that, there is a small bump in the estimation every time the quadrotor starts descending, and this is due to the fact that the quadrotor needs to decrease its thrust in order to start moving.

Fig. 9 gives another example of quadrotor landing on a table that is rolled underneath the vehicle as it is descending. The quadrotor detects the table and perform correctly an autonomous landing.

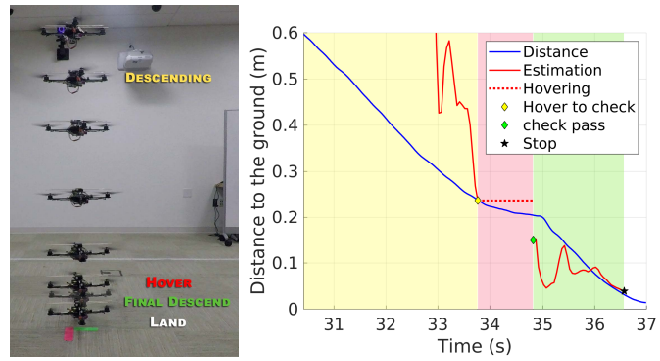

(a) (b)

Fig. 8. Experiment validation of an autonomous landing based on throttle reduction. Fig. 8b shows the real and estimated height as function of the time. The yellow,red, and green areas of the plot refers to stage 1,2,and 3 respectively.

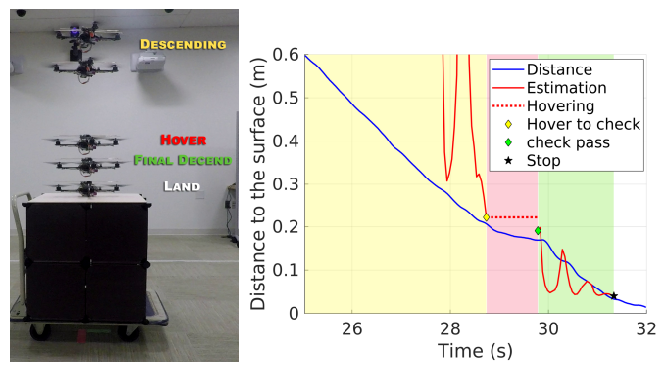

(a) (b)

Fig. 9. Experiment validation of an autonomous landing on a table by leveraging the ground effect. Fig. 9b shows the estimated distance during the landing.

VI. Energy Surface-based Path Planning

In the previous section, we provided evidence of thrust reduction given by the ground and ceiling effect to develop a sensorless autonomous surface detection. These results can furthermore be leveraged also for generating energy efficient trajectories near surfaces. Consider the problem of navigating an environment to reach a goal g while minimizing energy.

Ceiling, floors, and other flat surfaces can be exploited along the path to lower energy consumption through thrust reduction.

In this section, we solve *Problem 2* by proposing a path planning algorithm that modifies a generic path $P = \{p_0, p_1, \ldots, p_N, p_g\}$ into a directed-graph whose edges represent the energy cost required by the UAV to travel between two consecutive waypoints. The minimum energy path is computed by applying the well known Dijkstra's algorithm. The contribution of this section is twofold. We present: a) an energy model for calculating the weights of the graph edges that leverage the ground and ceiling effects and b) an algorithm that generates a directed-graph from a path P.

Authorized licensed use limited to: University of Virginia Libraries. Downloaded on February 19,2022 at 19:12:14 UTC from IEEE Xplore. Restrictions apply.

The approach is validated both in simulation and with real experiments.

A. Energy Model based on thrust/surface correlation

The objective of this section is to provide an energy model that will be used by the path planning algorithm to find the optimal path that minimizes energy consumption by leveraging surfaces if convenient.

Consider a quadrotor of mass m having four motors, two of them rotating clockwise while the others rotating counter-clockwise. Denoting the rotational speed of each propeller i by ω_i, it is possible to compute the thrust F_i and the torque T_i as:

$$F_i = k_f \omega_i^2,\ T_i = k_m \omega_i^2,\ i = 1, \cdots, 4 \tag{4}$$

where k_f and k_m are the proportionality constants for thrust and moment, respectively [14].

The quadrotor can be modeled as a 12th order state vector:

$$\boldsymbol{x} = \begin{bmatrix} \boldsymbol{p}_q^{\mathsf{T}} & \phi & \theta & \psi & v_x & v_y & v_z & \omega_x & \omega_y & \omega_z \end{bmatrix}^{\mathsf{T}}$$

where $\boldsymbol{p}_q = [x\ y\ z]^{\mathsf{T}}$ is the world frame position, v_x, v_y and v_z are the world frame velocities, ϕ, θ and ψ are the roll, pitch and yaw Euler angles and ω_x, ω_y and ω_z are the body frame angular velocities [12]. The dynamics of the quadrotor can be described as a nonlinear system of the form $\dot{\boldsymbol{x}} = f(\boldsymbol{x}, \boldsymbol{u})$ where $\boldsymbol{u}$ are the inputs of the systems and are given by:

$$\begin{bmatrix} u_1 \\ u_2 \\ u_3 \\ u_4 \end{bmatrix} = \begin{bmatrix} F \\ M_x \\ M_y \\ M_z \end{bmatrix} = \begin{bmatrix} k_f & k_f & k_f & k_f \\ 0 & Lk_f & 0 & -Lk_f \\ -Lk_f & 0 & Lk_f & 0 \\ k_m & -k_m & k_m & -k_m \end{bmatrix} \begin{bmatrix} \omega_1^2 \\ \omega_2^2 \\ \omega_3^2 \\ \omega_4^2 \end{bmatrix}. \tag{5}$$

The two components using power on the robot are the motors and the onboard electronics. We can omit the energy consumed by the electronics from our calculations since it is one order of magnitude less than the power used by the motors. The total power consumed by the quadrotor is equal to:

$$P = \sum_i^4 P_i \tag{6}$$

where $P_i = T_i \omega_i,\ i = 1, \cdots, 4$ is the power consumed by each motor. From eq.(4), it is possible to write the rotational speed w_i as:

$$w_i = \sqrt{\frac{F_i}{k_f}}. \tag{7}$$

Since the total thrust $F = \sum_i^4 F_i$,we can rewrite P as:

$$P = \sum_i^4 T_i \omega_i = \sum_i^4 k_m \omega_i^3 = k_m \sum_i^4 \left(\frac{F_i}{k_f}\right)^{\frac{3}{2}} = \frac{k_m}{k_f^{\frac{3}{2}}} \sum_i^4 F_i^{\frac{3}{2}} \tag{8}$$

$$= \frac{k_m}{k_f^{\frac{3}{2}}} \left[\sum_i^4 \left(\frac{F_i}{F} F\right)^{\frac{3}{2}}\right] = \left[\frac{k_m}{k_f^{\frac{3}{2}}} \sum_i^4 \left(\frac{F_i}{F}\right)^{\frac{3}{2}}\right] F^{\frac{3}{2}}. \tag{9}$$

If the quadrotor is not performing aggressive maneuvers, we can approximate $F_i = F/4$, thus we can deduct that the total power P is proportional to the squared cube of the thrust:

$$P \propto F^{3/2}. \tag{10}$$

To validate the assumption given in eq.(10), we performed an experiment in which we generated multiple trajectories at descending and ascending angles from 0 to 90 degrees as depicted in Fig. 10.

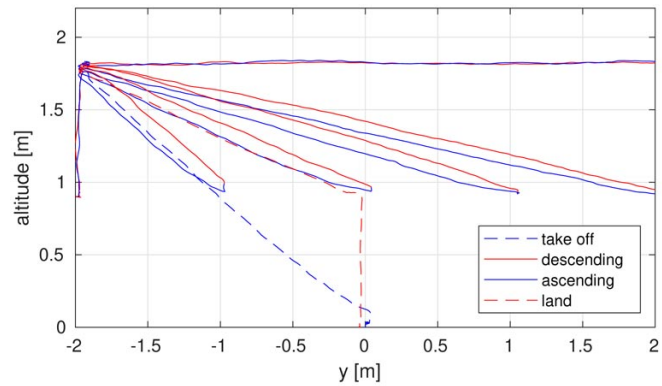

Fig. 10. Ascending and descending trajectories at different angles. For all the descending (ascending) paths the mean thrust is the same proving that they can be treated as descending(ascending) maneuvers.

For each trajectory, we analyzed the inputs $\boldsymbol{u}$ and the state $\boldsymbol{x}$ of the quadrotor as a function of time. Experiments highlighted that the throttle given to the quadrotor is overall constant during the same type of trajectory maneuver. Specifically, here we have considered three types of trajectory maneuver primitives: ascending, descending, and constant height flight.

In this way, it is possible to consider constant thrust when performing a maneuver as long as we can differentiate between different types of maneuvers. It is worth mentioning that, since the energy model will be used for comparing trajectories at the same speed, we can avoid modeling the aerodynamic effects due to drag forces that impact the power estimation as the speeds increases [15].

Table II summarizes the mean throttle measured when performing different maneuvers shown in Fig. 10. Thrust can be obtained as $\boldsymbol{F} = \boldsymbol{H}\boldsymbol{F}_{max}$ where $\boldsymbol{H}$ is the throttle in percentage and $\boldsymbol{F}_{max}$ is the maximum thrust which can be found in datasheets ($\boldsymbol{F}_{max} = 20$ N for the Hummingbird quadrotor). As expected, ascending requires more thrust than hovering, which in turn requires more thrust than descending. Note that the table also contains the throttle necessary to travel near-surface trajectories at a fixed distance, computed using the ground and ceiling models proposed in Section IV. d_∞, in this case, refers to a distance large enough such that ground and ceiling effects are negligible.

B. Path Planning

Given a path $P = \{p_0, p_1, \ldots, p_N, p_g\}$ consisting of N intermediate waypoints with p_0 the starting point and p_g the final goal and $S = \{s_1, s_2, \ldots, s_M\}$ the set of M surfaces along the path, we propose an algorithm for generating a directed graph to find the optimal path. Each edge of the directed graph has a cost that will be computed by using the energy model proposed in the previous section.

Authorized licensed use limited to: University of Virginia Libraries. Downloaded on February 19,2022 at 19:12:14 UTC from IEEE Xplore. Restrictions apply.

TABLE II

MEAN THRUST AT DIFFERENT MANEUVERS

Maneuver	Mean Throttle
Ascending	39.95%
Descending	39.60%
Hovering at d_∞	39.78%
Hovering at $d = 10$ cm from ceiling	37.00%
Hovering at $d = 5$ cm from ground	36.34%

In order to build the graph, we transform the waypoints, and the surface edges from a 3D-space into a 2-Dimensional space (x, z), where x represents the distance traveled along the path. Then, we slice the 2D space into a grid.

For the horizontally slicing, the grid is divided into $M + 1$ layers, each of them corresponding to the height of an available surface along the route, plus a mid-air layer. The upper side and underneath side of an object along the path are considered as two different surfaces. For vertical slicing, the grid is divided using all the waypoints and surface edges. If two or more horizontal/vertical layers are coincident (e.g., two surfaces at the same height), only one is considered.

The following rules are used to compute the vertices and the edges of the graph:

1) A vertex is a point given by the intersection between horizontal and vertical layers.
2) Any vertex can be connected only to vertices in the same or next vertical layer.
3) An edge connection between two consecutive vertices is removed from the graph if it intersects with an obstacle located between the two vertices.

The energy cost associated with each edge $E_{i,j}$ is then calculated as:

$$E_{i,j} = \hat{F} \cdot \frac{d_{i,j}}{|\overline{v}_{i,j}|} \tag{11}$$

where $E_{i,j}$ denotes the energy cost from v_i to v_j, $\hat{F}$ is the mean throttle, $d_{i,j}$ represents the distance between v_i and v_j and the $|\overline{v}_{i,j}|$ indicates the average speed of the quadrotor traveling from v_i to v_j. Depending on the type of maneuver to perform, the mean throttle $\hat{F}$ assumes different values derived from the energy model computed in the previous section and summarized in Table II.

Once the directed graph (G, V, E) is computed, we can use a Dijkstra algorithm [16] to find the shortest path from the starting vertex to the end vertex. Please note that the shortest energy path is not necessary the shortest distance path but the one that consumes the least energy by leveraging the ground and ceiling effects.

To clarify the proposed approach, we consider the example in Fig. 11 which is also the experimental case study presented next. This example shows a path composed of 4 waypoints $P = \{A, B, C, D\}$. The quadrotor is tasked to go from point A, starting at a certain height at the mid-air level (v_1), to point D in which is required to land, visiting each intermediate waypoint (B and C) at any height.

There are four surfaces ($M = 4$) along the path: a shelf, a table, an two floor sections (from v_4 to v_{20} and from v_{24} to v_{32}). The upper side of the shelf and the underneath side of the table are not included in the surface set because they are assumed not usable due to the presence of obstacles.

Following the rules outlined above, if for example the quadrotor is in v_{19}, it can only move to v_{17}, v_{18}, v_{20} along the same vertical layer or move to v_{21}, v_{22}, v_{23} in the next vertical layer. In the generated graph, we decided to avoid connecting a vertex to previous vertical layers because the goal is to get to the final destination while minimizing energy.

A typical path to complete this mission that does not decompose the space into multiple horizontal layers requires the UAV to follow the trajectory $V_{basic} = \{v_i | i = \{1, 5, 9, 13, 17, 21, 25, 29, 32\}\}$. If we compute the shortest path on the graph G using Dijkstra and the distance as a weight, we obtain the shortest distance path $V_{shortest} = \{v_i | i = \{1, 6, 11, 15, 19, 23, 28, 32\}\}$.

If instead, we consider our approach that leverage the ground and ceiling effects, the optimal path is not obvious. The minimum energy path obtained with our approach was found to be $V_{Optimal} = \{v_i | i = \{1, 6, 10, 15, 19, 23, 28, 32\}$. However, if the initial position was v_4, it would be better to leverage the path by visiting $v_i | i = \{4, 8, 12, 16, 19, 23, 28, 32\}$. Instead, when starting from v_3, if the nearby surfaces ($E_{6,10}$ or $E_{8,12}$) are not very long, it would be better just to stay at the current height and visit $v_i | i = \{3, 7, 11, 15, 19, 23, 28, 32\}$.

C. Results

We performed multiple experiments on the scenario illustrated in Fig. 11. The experiment setup and implementation is shown in Fig. 12.

The path is designed in an "U" shape. Two intermediate waypoints are at each of the corners of the U shape. A 0.9 m $\times$1.8 m transparent PVC board is set at 1.14 m above the ground as the shelf. The table (0.9 m $\times$1.8 m $\times$0.6 m) is between B, and C. Most of the ground surface is available except the part under the table. Four different cases were tested: 1) a basic path in which the quadrotor starts from A travels at mid-air through the intermediate waypoints and lands in D (Fig 13a); 2) the shortest distance path computed using the distances between vertices as edge weights (Fig 13b); 3) the minimum energy path computed with our approach (Fig 13d); and 4) the minimum energy path computed with our approach, but in a scenario without two of the surfaces (Fig 13c).

The first path is chosen since it is the most intuitive way to operate if the surrounding environment is not exploited. The second path is the one that is typically used since it aims at minimizing the travel distance. The third path is the one that leverages the surrounding surfaces to minimize energy consumption while the last one is used for comparison purpose.

For each experiment, we performed five flights in which we measured the total throttle given to the quadrotor. Note that, given eq.(10), the total thrust is proportional to the total energy:

$$\hat{E}_{Traj} = \int P dt \propto \int F^{3/2} dt. \tag{12}$$

For ease of discussion, here we will use the last term on the right-hand side of eq.(12) to compute the total energy during a trajectory since we can measure the throttle provided to the UAV.

Authorized licensed use limited to: University of Virginia Libraries. Downloaded on February 19,2022 at 19:12:14 UTC from IEEE Xplore. Restrictions apply.

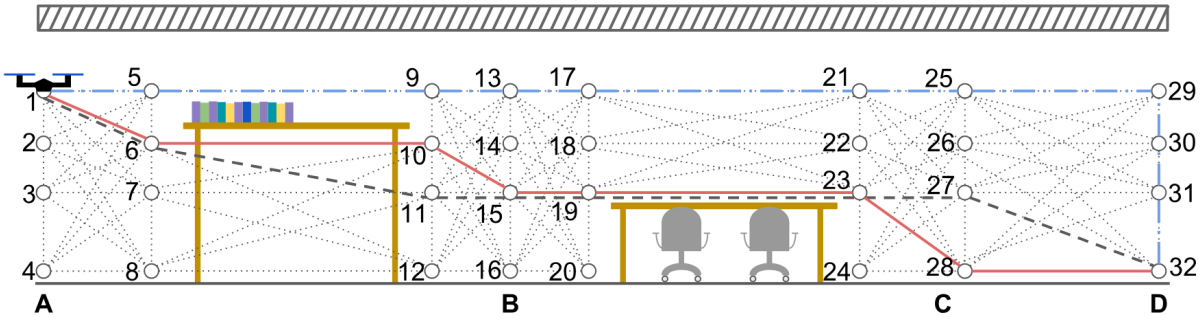

Fig. 11. Generated graph from a path $P = \{A, B, C, D\}$, a shelf, a table, and two free floor sections. The dotted dashed line (blue) highlights a basic path that would be performed without decomposing it into a graph. The solid line (red) represents the minimum energy optimal path while the dashed line (black) indicates the shortest distance path.

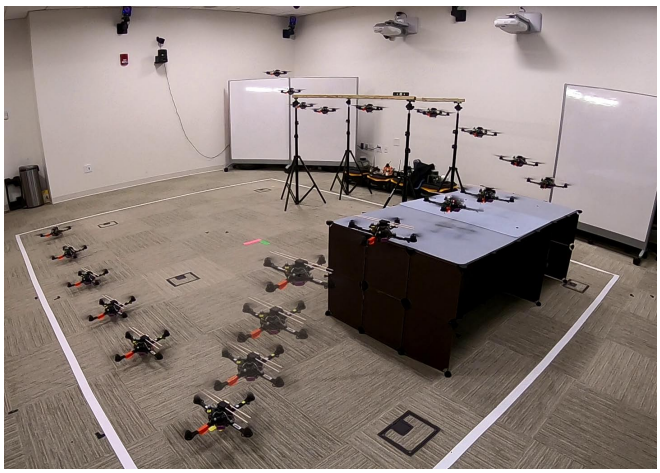

Fig. 12. Snapshot of one run of the minimum-energy optimal path. The path represented in Fig. 11 is reproduced as a U Shape. The UAV flies below a transparent PVC board, above a table, and close to the ground.

Fig. 14 compares the throttle between the basic path and the optimal path. We can see a significant thrust reduction for the optimal path. The optimal path consumes 15.86% less energy and also takes less time. The figure also shows three dashed rectangles highlighting the average throttle reduction given by traveling close to the surfaces.

Fig. 14b compares the throttle between the optimal path and the same path but without the shelf and the table surfaces. This comparison highlights the throttle reduction that appears when the UAV flies underneath the shelf and above the table. In fact, the same path without the surfaces consumes about 4% more.

Finally, Fig. 13b compares the shortest distance path with our approach. Although the shortest path travels a shorter distance and takes less time to complete the mission, our approach still consume less energy.

Table III summarizes the total energy computed using eq.(12) for both the simulation and the actual experimental trials. For the experiments, we provide the mean value and standard deviation over five executions.

It is possible to see that the total measured throttle during the real flights is very close to the predicted one, confirming the effectiveness of our energy model. The slight difference between the values is due to noise, modeling errors, and the fact that the actual distance of the UAV from the surface may be different from the fixed value chosen for computing the edges (Table II).

TABLE III

EXPERIMENT RESULTS OF PREDICTED AND MEASURED ENERGY*

Path	Predicted total energy	Measured total energy	
		mean	*std*
Basic path	13.0843	13.3168	0.0221
Shortest path	11.2445	11.5944	0.0289
Optimal path	10.7906	11.2050	0.0111
Optimal path (no surfaces)	11.2622	11.6627	0.0587

$*$ The energy consumption is estimated as a function of the throttle.

VII. Conclusions and Future Work

In this work, we have developed an approach that enables UAVs to leverage ground and ceiling effects in order to detect surfaces and achieve energy efficient path planning. Our results indicate that distances to surfaces can be efficiently detected and estimated by monitoring the thrust provided to the system without the need for other sensors. The same effects can be leveraged to minimize energy consumption by planning trajectories that enable the UAV to fly near ground and ceiling surfaces. To this end, we have constructed a model for energy consumption and a graph-based approach to compute the minimum energy trajectory for a UAV tasked to navigate through multiple points along a path. Extensive experiments have been presented to validate the proposed UAV thrust model, the surface detection approach, and energy-aware path planning technique. On the latter, we demonstrated that it is possible to save about 10% energy when flying in proximity to surfaces during autonomous operations.

Future extensions of the proposed work will consider the characterization of flow dynamics effects in tight formations of UAV swarms and more complicated scenarios such as detection and landing on moving vehicles and more aggressive maneuvers of the vehicles near surfaces.

Acknowledgment

This material is based upon work supported by NSF under grant#1816591 and the Air Force Research Laboratory (AFRL) and the Defense Advanced Research Projects

Authorized licensed use limited to: University of Virginia Libraries. Downloaded on February 19,2022 at 19:12:14 UTC from IEEE Xplore. Restrictions apply.

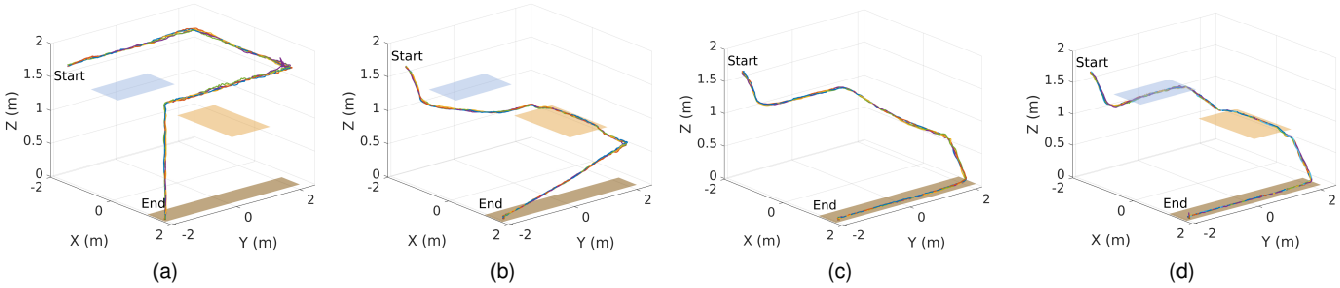

Fig. 13. The experiment trajectories for (a) basic path, (b) optimal path, (c) optimal path without the shelf and the table, and (d) shortest path.

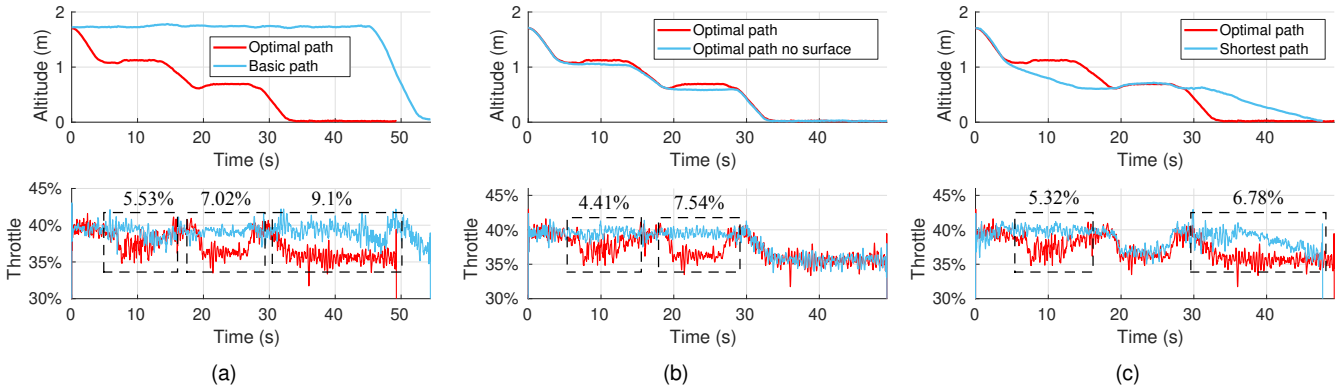

Fig. 14. (a) The quadrotor needs less thrust when it is close to the shelf, table, and the ground surfaces. The optimal path consumes 15.86% less energy than the basic path. (b) The quadrotor has clear thrust reduction when it is close to the shelf and the table comparing with the one without these surfaces. These two experiments have the same trajectories. (c) Although the optimal path is longer than the shortest path, it is less energy-consuming due to the throttle reduction obtained when the quadrotor is flying near the surfaces. The throttle reduction is marked with a black box.

Agency (DARPA) under Contract No. FA8750-18-C-0090. Any opinions, findings and conclusions or recommendations expressed in this material are those of the authors and do not necessarily reflect the views of AFRL, DARPA, the Department of Defense, or the United States Government.

References

[1] I. Cheeseman and W. Bennet, "The effect of the ground on a helicopter rotor," *R & M*, vol. 3021, 1957.

[2] S. A. Conyers, M. J. Rutherford, and K. P. Valavanis, "An empirical evaluation of ceiling effect for small-scale rotorcraft," in *2018 International Conference on Unmanned Aircraft Systems (ICUAS)*. IEEE, 2018, pp. 243–249.

[3] I. Sharf, M. Nahon, A. Harmat, W. Khan, M. Michini, N. Speal, M. Trentini, T. Tsadok, and T. Wang, "Ground effect experiments and model validation with draganflyer x8 rotorcraft," in *2014 International Conference on Unmanned Aircraft Systems (ICUAS)*. IEEE, 2014, pp. 1158–1166.

[4] A. Kushleyev, D. Mellinger, C. Powers, and V. Kumar, "Towards a swarm of agile micro quadrotors," *Autonomous Robots*, vol. 35, no. 4, pp. 287–300, 2013.

[5] Y. H. Hsiao and P. Chirarattananon, "Ceiling effects for surface locomotion of small rotorcraft," in *2018 IEEE/RSJ International Conference on Intelligent Robots and Systems (IROS)*. IEEE, 2018, pp. 6214–6219.

[6] P. Sanchez-Cuevas, G. Heredia, and A. Ollero, "Characterization of the aerodynamic ground effect and its influence in multirotor control," *International Journal of Aerospace Engineering*, vol. 2017, 2017.

[7] ——, "Multirotor uas for bridge inspection by contact using the ceiling effect," in *2017 International Conference on Unmanned Aircraft Systems (ICUAS)*. IEEE, 2017, pp. 767–774.

[8] C. Powers, D. Mellinger, A. Kushleyev, B. Kothmann, and V. Kumar, "Influence of aerodynamics and proximity effects in quadrotor flight," in *Experimental robotics*. Springer, 2013, pp. 289–302.

[9] S. Shen, N. Michael, and V. Kumar, "Autonomous multi-floor indoor navigation with a computationally constrained mav," in *2011 IEEE International Conference on Robotics and Automation*. IEEE, 2011, pp. 20–25.

[10] A. Cesetti, E. Frontoni, A. Mancini, P. Zingaretti, and S. Longhi, "A vision-based guidance system for uav navigation and safe landing using natural landmarks," *Journal of intelligent and robotic systems*, vol. 57, no. 1-4, p. 233, 2010.

[11] A. Gautam, P. Sujit, and S. Saripalli, "A survey of autonomous landing techniques for uavs," in *2014 international conference on unmanned aircraft systems (ICUAS)*. IEEE, 2014, pp. 1210–1218.

[12] N. Bezzo, K. Mohta, C. Nowzari, I. Lee, V. Kumar, and G. Pappas, "Online planning for energy-efficient and disturbance-aware uav operations," in *2016 IEEE/RSJ International Conference on Intelligent Robots and Systems (IROS)*. IEEE, 2016, pp. 5027–5033.

[13] C. Di Franco and G. Buttazzo, "Coverage path planning for uavs photogrammetry with energy and resolution constraints," *Journal of Intelligent & Robotic Systems*, vol. 83, no. 3-4, pp. 445–462, 2016.

[14] D. Mellinger, M. Shomin, and V. Kumar, "Control of quadrotors for robust perching and landing," in *Proceedings of the International Powered Lift Conference*, 2010, pp. 205–225.

[15] Z. Liu, R. Sengupta, and A. Kurzhanskiy, "A power consumption model for multi-rotor small unmanned aircraft systems," in *2017 International Conference on Unmanned Aircraft Systems (ICUAS)*. IEEE, 2017, pp. 310–315.

[16] E. W. Dijkstra, "A note on two problems in connexion with graphs," *Numerische mathematik*, vol. 1, no. 1, pp. 269–271, 1959.

Authorized licensed use limited to: University of Virginia Libraries. Downloaded on February 19,2022 at 19:12:14 UTC from IEEE Xplore. Restrictions apply.